Backscattering in antiresonant hollow-core fibers: over 40 dB lower than in standard optical fibers - Supplemental document

V. Michaud-Belleau[1], E. Numkam Fokoua[2], T. D. Bradley[2], J. R. Hayes[2], Y. Chen[2], F. Poletti[2], D. J. Richardson[2], J. Genest[1], and R. Slavík[2,*]

[1] Centre d'optique, photonique et laser, Université Laval, Québec, QC, G1V 0A6, Canada
[2] Optoelectronics Research Centre, University of Southampton, Southampton, SO17 1BJ, UK
[*] Corresponding author: r.slavik@soton.ac.uk

Compiled January 4, 2021

This document provides supplementary information to "Backscattering in antiresonant hollow-core fibers: over 40 dB lower than in standard optical fibers", http://dx.doi.org/10.1364/optica.XX.XXXXXX. Here, we present the OFDR instrument in further detail, justifying some of the design choices and describing its most important modules, and give information about the NANF sample. We also outline the steps taken to correct and calibrate the raw data and explain how the detection sensitivity is calculated and optimized.

http://dx.doi.org/10.1364/optica.XX.XXXXXX

Instrument. Figure S1 depicts the instrument in a format that is different from that shown in the Letter. The stable laser is an OE-Waves WGM Gen3 with 195 THz mean frequency (1539.8 nm) and 7 mW output power. To produce an approximately linear chirp through modulation, a triangular waveform is chosen instead of a sawtooth waveform; this avoids exciting the high-frequency resonances measured in the laser's FM response. The reference interferometer (shown in the Letter) is based on the Mach-Zehnder configuration with balanced quadrature detection [1] (Kylia COH24 optical 90° hybrid). It is characterized by a $\tau_{ref} = 494.95$ ns differential delay (≈ 100 m, Fujikura SM15-PS-U25A fiber) which was measured with a commercial OFDR instrument. The Mach-Zehnder format minimizes the contamination by Rayleigh scattering produced within the reference interferometer while quadrature detection simplifies the measurement of the chirp polarity given the triangular modulation waveform. The 27 MHz frequency shift is produced by a Gooch & Housego R26027-2-1-1.55-LTD-FO-FC/APC AOM with a 3 dB insertion loss. Frequency-shifting is necessary to suppress offending self-mixing terms and excess low-frequency digitizer noise, but it also mitigates the impact of the undesirable relative intensity noise (RIN) of the laser as well as that of the crosstalk between the acquisition channels. The balanced photodetector is a Thorlabs PDB430C with a 5.00 V/mA transimpedance gain, a 0.8 quantum efficiency, a 350 MHz bandwidth, and a 7 pW/Hz$^{1/2}$ noise-equivalent power (NEP). All signals are sampled at 125 MS/s with a GaGe CSE8389 14-bit digitizer (10.6 ENOB in operation) after appropriate anti-aliasing filtering with Mini-Circuits BLP-1.9+ or BLP-50+ low pass filters. For convenience, an inline PC (Thorlabs, CPC250) is used on the already bare input pigtail, but other positions would have been possible.

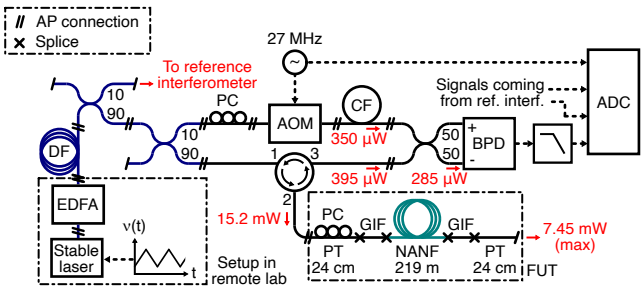

Fig. S1. Partial layout of the OFDR. EDFA, erbium-doped fiber amplifier; DF, delay fiber; PC, polarization controller; AOM, acousto-optic modulator; CF, compensation fiber; BPD, balanced photodetector; ADC, analog-to-digital converter (digitizer); PT, pigtail; GIF, graded-index fiber; FUT, fiber under test. Solid lines represent fibers (black is standard, blue is polarization maintaining) and dashed lines represent electrical cables.

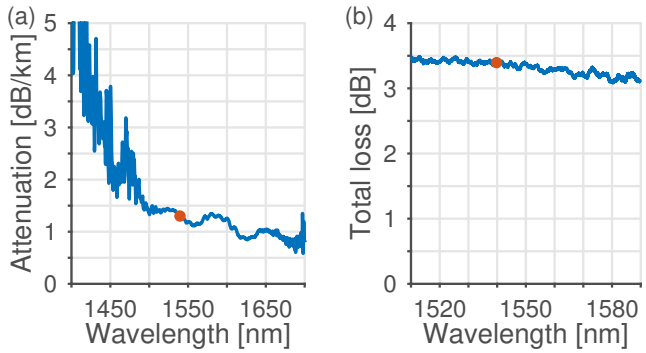

Fig. S2. Loss characterization of the NANF (version used for this demonstration). (a) Spectral attenuation of the fiber, measured via cutback from 570 to 10 m. (b) Total transmission loss of the 219-m pigtailed sample, measured using an amplified spontaneous emission source and optical spectrum analyzer.

NANF sample. The fiber used in the experiments was fabricated using the same stack, fuse, and two-stage draw process reported in [2]. It was drawn to a core diameter of approximately 35 µm and an average cladding membrane thickness of approximately 550 nm. To measure the NANF's loss, we butt coupled an endlessly single-mode photonic crystal fiber (with a closely matched mode field diameter) to its input and performed a cutback transmission measurement from 570 m to 10 m. Figure S2(a) depicts the measured attenuation between 1400 and 1700 nm, showing 1.2 dB/km near 1550 nm and 1.3 dB/km at the operating wavelength of our OFDR (1539.8 nm). We note that, because of the short cutback length, the loss of the fundamental mode may yet be lower than these measured values. As described in [2], the loss of the fiber has contributions from leakage, microbending, and surface scattering (the loss peaks around 1450 nm are due to water vapor absorption in the air core). Leakage loss is dominant in NANF, but only scattering contributes to the BSC. Therefore, unlike in SMF and HC-PBGF for which scattering loss is typically dominant, the loss in NANF is not directly proportional to the BSC. The total transmission loss of the 219-m pigtailed NANF sample, dominated by loss at the interconnections (see main text), was also measured from 1510 to 1590 nm (Fig. S2(b)).

Correction and calibration. For the specific case of a single static reflection occurring within the NANF sample (reflectivity ρ, delay τ with respect to the signal in the reference arm) and for a single infinite sweep of the laser, the voltage signal produced by the measurement interferometer can be expressed as:

$$V(t) = V_0 \rho \cos\left[2\pi\gamma\tau t + \theta_{las}(t,\tau) + \theta_{aom}(t) + \theta_0\right] + n(t), \tag{S1a}$$

$$V_0 = 2G\mathcal{R}k_c\sqrt{k_s P_{fut} P_{LO}}, \tag{S1b}$$

where $\theta_{las}(t,\tau)$ is the phase error due to a combination of laser phase noise and chirp nonlinearity, both scaling with τ (more rigorously, they are filtered by a τ-dependent impulse response [3]), $\theta_{aom}(t)$ is the phase signal introduced by the AOM, a phase ramp with slope $2\pi f_{aom}$ contaminated by phase noise from the driving synthesizer, θ_0 is a phase offset, and $n(t)$ is the additive measurement noise. The calibration factor k_c accounts for excess loss in the 3-dB output coupler as well as for a small attenuation that is voluntary applied to attain an optimal power balance at the photodetector. Similarly, the calibration factor k_s accounts for the 1.1 dB loss of the circulator (return path from pigtail 2 to 3) and for the 1.6 dB loss of the interconnection between the NANF and its input SMF pigtail. Other parameters are defined in Table S1 along with the numerical values used in this work.

Table S1. Parameters used to normalize the photovoltage and compute the shot-noise-limited sensitivity.

Parameter	Description	Value	Units
γ	Average chirp rate	93.5	GHz/s
G	Transimpedance gain	5.00	V/mA
$\mathcal{R}$	Responsivity	1.00	A/W
k_c	Coupler calibration factor	0.78	-
k_s	Sample calibration factor	0.38	-
P_{fut}	Power sent to FUT	15.2	mW
P_{LO}	Power in reference arm	350	µW
ν_0	Laser frequency	195	THz
P_s	Power in sample arm	395	µW
η_q	Quantum efficiency	0.80	-
n	Group index	1.00	-

To properly estimate the values of ρ and τ of a single reflection, several corrections are applied in post-processing. First, from an estimate of $\theta_{aom}(t)$ obtained through the simultaneous acquisition of the signal driving the AOM, a phase correction is applied on a sampled version of the signal defined in Eq. S1a (also compensating for the delay caused by the acoustic wave propagation in the AOM, measured to be 1.46 µs). This shifts the signal to baseband and removes the phase noise introduced by the synthesizer, but it also adds some noise because the estimation of $\theta_{aom}(t)$ is performed with a finite signal-to-noise ratio. Then, a resampling operation is implemented using information extracted from the reference interferometer (Fig. S3). This suppresses the phase error $\theta_{las}(t,\tau)$, though the cancellation is only complete for $\tau = \tau_{ref}$ [3]. Finally, the phase-corrected and resampled signal is normalized by V_0 (Eq. S1b); this number is computed from calibration data taken right after the digitization of $V(t)$ (Eq. S1a).

All those operations yield a signal approaching the ideal form of $\rho\cos(2\pi\gamma\tau t + \theta_0)$, though in practice it is sampled, corrupted by noise, and only available over a finite duration T determined by the sweep bandwidth Δf ($T = \Delta f/\gamma$). The tools of spectral analysis can then be deployed to estimate ρ and τ with the usual trade-off between resolution and dynamic range. The case of a distributed reflection along the fiber (backscattering) is treated in the same way and with the same calibration values, though the spectral analysis is adapted to perform the estimation of a PSD instead of the Fourier series appropriate for discrete reflections. This PSD can then be converted to the desired reflectance density using the conversion factor $2n\gamma/c$ in Hz/m (the same factor is used to convert the frequency axis to a range axis [4]), using the value of γ extracted from the reference interferometer data. Barring contamination by discrete reflections or measurement noise, the level of this reflectance density is a property of the fiber and does not depend on the instrument's settings.

Since 200 laser sweeps are recorded when the memory of the digitizer is filled, it is worth stating that the phase correction and the V_0 normalization are performed over the full signal while

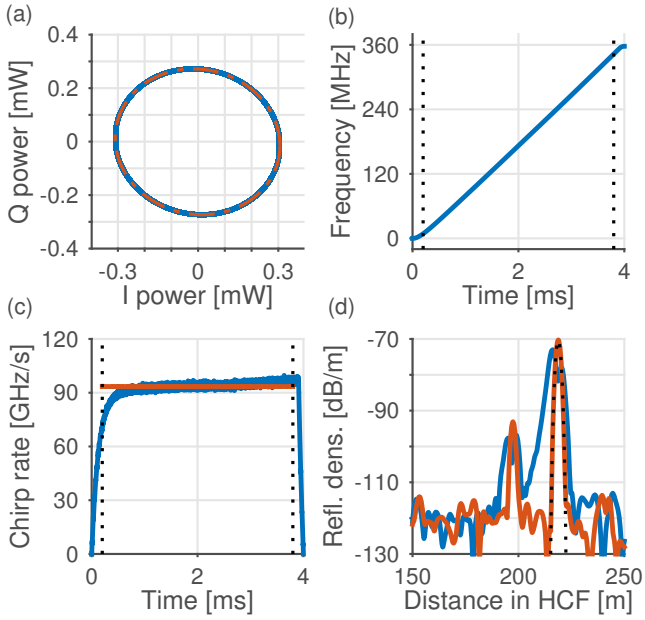

Fig. S3. Resampling operation. (a) IQ signal produced by the reference interferometer. The blue curve is the data, the dashed orange curve is the elliptical fit. (b) Frequency signal extracted from the interferometric phase (low-frequency conversion gain $2\pi\tau_{ref}$). The dotted black lines delineate the segment kept for spectral analysis. (c) Instantaneous chirp rate. The blue curve is the derivative of the curve in (b), the orange curve is its resampled version. (d) Comparison of the reflectance density obtained with (orange) and without (blue) resampling of the measurement interferometer's signal for a single laser sweep. The dotted black line represents the transform of the Kaiser window (β =12) used for spectral analysis, illustrating that the resampled signal is transform-limited.

the resampling is done sweep by sweep, taking the switching polarity of the chirp into account. After the resampling, temporal averaging and spectral averaging (of PSDs) can be traded as desired since the scattering signal is repeatable from sweep to sweep when it originates from static surface roughness.

Sensitivity. The additive measurement noise $n(t)$ in Eq. S1a is a sum of several zero-mean contributors and can be described through its one-sided PSD, $S_n^{(1)}(f)$. Since the phase correction and the resampling operation have negligible impact over broadband white noise, and since all the relevant contributors to $n(t)$ are approximately white around $f_{aom} = 27$ MHz, it is appropriate to base the following calculations on the PSD level at this frequency. Considering the normalization by V_0 and the conversion from a frequency density to a spatial density, the measurement noise is described by the following uniform single-sweep sensitivity or noise-equivalent reflectance density (in m^{-1}):

$$R_n = \frac{2S_n^{(1)}(f_{aom})}{V_0^2}\frac{2n\gamma}{c}, \tag{S2}$$

where the factor of 2 in the first term accounts for the effect of the cosine in Eq. S1a. For example, the shot noise contribution (in units of V^2/Hz) can be calculated as [5]:

$$S_{n,sn}^{(1)}(f_{aom}) = (G\mathcal{R})^2\,\frac{2h\nu_0 k_c\,(P_s + P_{LO})}{\eta_q}, \tag{S3}$$

where P_s is the power measured in the sample arm when the polarization controllers are adjusted to minimize the contribution of the remote splice at 219 m. From the values found in Table S1, the shot-noise-limited sensitivity can be evaluated to be −133 dB/m. Similarly, a detector-noise-limited sensitivity of −139 dB/m can be computed from the given NEP. Other contributors to the sensitivity include the digitizer noise, laser RIN coupling through the first splice reflection, and noises introduced by the phase correction and resampling operation.

Equation S2 illustrates that the sensitivity can be improved (that the noise floor can be lowered) by decreasing the chirp rate γ. This explains why our instrument is operated at a relatively low chirp rate with respect to a typical OFDR. Although it would be possible to further decrease γ, we found that the laser phase noise couples efficiently through the signal that does two round-trips in the fiber (three reflections at the interconnections, remote-local-remote, for a total delay $\tau_3 \approx 2.9$ µs). This signal is roughly 10 dB stronger than the signal coming from the remote splice (one reflection) which is better polarization-cancelled. Considering that the phase noise gain scales with the delay [4], this signifies that the phase noise around the parasitic tone at 438 m is approximately 16 dB stronger than that of the tone around 219 m, and its impact has to be mitigated through adjustment of the chirp rate. We found that $\gamma \approx$ 80-500 GHz/s was an appropriate range of operation to avoid significant phase noise contamination: from Fig. S4(a), the most quiet spectral range is between 120 kHz and 1.45 MHz, so we impose $\gamma\tau_3 < 1.45$ MHz to bring the high-frequency tones at a negative range, and $\gamma\tau_3/2 > 120$ kHz to bring the low-frequency noise beyond the end of the backscattering range (Fig S4(b-c)).

In a similar manner, an inspection of Eq. S3 can justify our choice of input coupling ratio: to operate the photodetector close to saturation, the product $P_s P_{LO}$ must be kept constant. Given this constraint, the shot noise contribution is minimized when $P_s = P_{LO}$, a condition that we have tried to reach first by using a 90:10 input coupler, but also by using a custom-made EDFA to adjust the overall power (this EDFA is installed in another lab to minimize the pick-up of its acoustic noise). Amplification to 20 mW is sufficient with this NANF sample, though this leads to a higher RIN and a penalty in sensitivity compared to the case in which the laser would have sufficient output power [5]. Finally, the fine tuning of the balancing was done by inserting a fixed attenuator at the end of the compensation fiber (not shown in Fig S1). This compensation fiber is used so that the condition $\tau = 0$ occurs approximately at the input splice of the FUT, nulling as much of the associated phase noise as possible.

Figure S4(d) shows the reflectance density of a 200-m sample of SMF-28 terminated by angled physical contact (APC) connectors. For this verification measurement, the OFDR instrument was slightly modified: an optical 90° hybrid was used instead of the usual AOM. The signal observed between -200 and 0 m is the partially suppressed (by roughly 37 dB) negative copy of the scattering signal between 0 and 200 m, a consequence of the imperfections of the optical hybrid. This constitutes another reason why the AOM was used for the purpose of NANF characterization. The cutoff seen around 650 m, on the other hand, is due to a digital filter which is not apparent in the NANF measurements because of its lower effective index. Weak reflections from the APC connectors are visible at 0 and 200 m, as expected, while the measurement noise floor sits at approximately −125 dB/m (single-sweep sensitivity at $\gamma = 184$ GHz/s). This is slightly different from the −124 dB/m single-sweep sensitivity measured for NANF at $\gamma = 184$ GHz/s, a reasonable discrepancy given

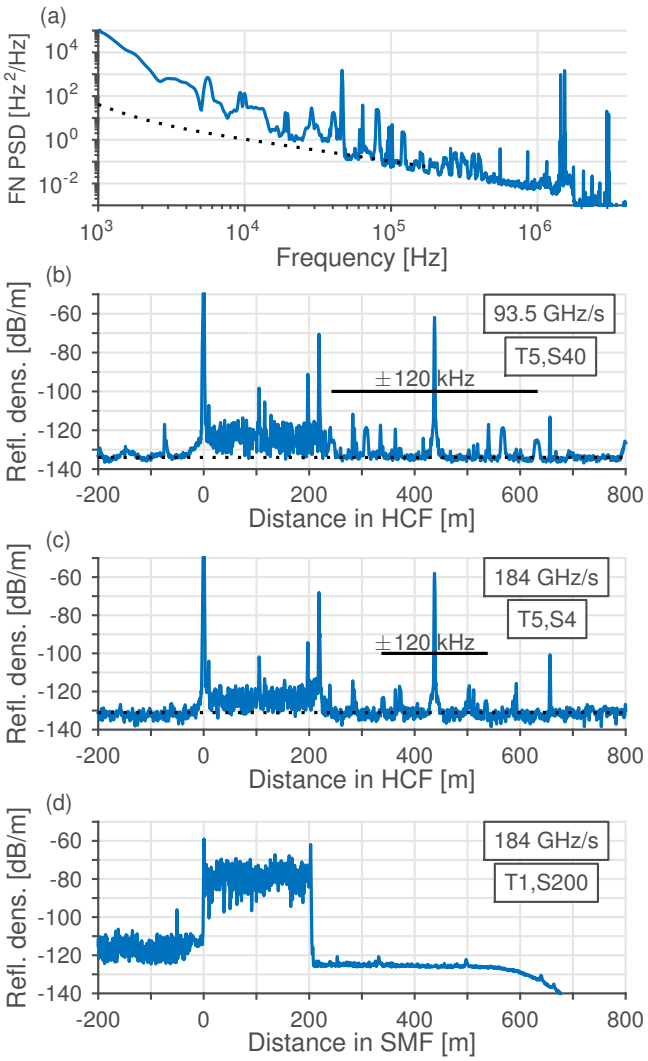

Fig. S4. (a) One-sided frequency noise (FN) PSD of the laser in operation. The dotted black line is representative of the PSD when the laser is not modulated; the low-frequency excess noise and the tones between 40 and 120 kHz are produced by the driving synthesizer (a low pass filter with cutoff frequency 100 kHz is used at the modulation input to attenuate this noise). (b) Measured reflectance density in NANF, extended beyond the scattering range to show the signal at 438 m caused by the triple reflection along with the associated sidebands. The solid black line delimits the region where laser noise contamination due to this triple reflection is most problematic. The dotted black line is the noise floor. (c) Same for a higher chirp rate, showing the compression of the laser noise sidebands but higher additive noise floor. (d) Reflectance density of a 200-m SMF sample terminated by APC connectors, measured with a slightly modified OFDR instrument.

the higher refractive index in SMF, lower return power due to interconnections (lower shot noise and RIN), as well as the slightly modified optical setup (no loss from the AOM, no phase correction). Yet, this measurement shows that the custom-built OFDR instrument, though highly optimized for the characterization of this specific NANF sample, still maintains an outstanding sensitivity for other fiber samples.

REFERENCES

1. V. Michaud-Belleau, H. Bergeron, P. Light, N. Hébert, J. Deschênes, A. Luiten, and J. Genest, "Passive coherent discriminator using phase diversity for the simultaneous measurement of frequency noise and intensity noise of a continuous-wave laser," Metrologia **53**, 1154 (2016).
2. G. T. Jasion, T. D. Bradley, K. Harrington, H. Sakr, Y. Chen, E. N. Fokoua, I. A. Davidson, A. Taranta, J. R. Hayes, D. J. Richardson, and F. Poletti, "Hollow core NANF with 0.28 dB/km attenuation in the C and L bands," in *Optical Fiber Communication Conference,* (Optical Society of America, 2020), pp. Th4B–4.
3. X. Fan, Y. Koshikiya, and F. Ito, "Phase-noise-compensated optical frequency domain reflectometry with measurement range beyond laser coherence length realized using concatenative reference method," Opt. Lett. **32**, 3227–3229 (2007).
4. S. Venkatesh and W. V. Sorin, "Phase noise considerations in coherent optical fmcw reflectometry," J. Light. Technol. **11**, 1694–1700 (1993).
5. R. Hui and M. O'Sullivan, *Fiber optic measurement techniques* (Academic Press, 2009).